Ab initio relativistic configuration interaction calculations of the spectrum of bismuth oxide: Potential curves and transition probabilities

Aleksey B. Alekseyev, HeinzPeter Liebermann, Robert J. Buenker, Gerhard Hirsch, and Yan Li

Citation: The Journal of Chemical Physics **100**, 8956 (1994); doi: 10.1063/1.466700
View online: http://dx.doi.org/10.1063/1.466700
View Table of Contents: http://scitation.aip.org/content/aip/journal/jcp/100/12?ver=pdfcov
Published by the AIP Publishing

Ab initio relativistic configuration interaction calculations of the spectrum of bismuth oxide: Potential curves and transition probabilities

Aleksey B. Alekseyev,[a] Heinz-Peter Liebermann, Robert J. Buenker, Gerhard Hirsch, and Yan Li

Bergische Universität, Gesamthochschule Wuppertal, Fachbereich 9, Theoretische Chemie, Gaussstrasse 20, D 42097 Wuppertal, Germany

(Received 3 January 1994; accepted 2 March 1994)

A series of configuration interaction calculations employing relativistic effective core potentials including the spin–orbit interaction is reported for the $X_1\ ^2\Pi_{1/2}$ ground and numerous low-lying excited states of the bismuth oxide molecule up to 30 000 cm^{-1}. Special difficulties connected with the treatment of open-shell systems and double-group irreducible representations are discussed and a feasible computation scheme is developed for dealing with them. The spin–orbit interaction is found to cause a high level of mixing between a variety of low-lying $\lambda-s$ states, producing a number of avoided crossings which play a key role in determining the character of the BiO spectrum. A comparison with existing experimental data for both the energy locations and intensities of a large number of band systems indicates that the present calculations are capable of predicting T_e values to an accuracy of 0.1–0.2 eV. Corresponding radiative lifetime results generally agree within a factor of 2, with the best experience occurring for relatively strong transitions. The state which was originally assigned as $A\ ^2\Pi_{1/2}$ actually turns out to be dominated by the $^4\Pi$ $\lambda-s$ state. The corresponding state with $\Omega=3/2$ has recently been discovered by Fink and Shestakov and is found to undergo a strong nonadiabatic interaction with the $X_2\ ^2\Pi_{3/2}$ state. Two other related states $A_3\ ^4\Pi_{5/2}$ and $A_4\ ^4\Pi_{1/2}$ are predicted by the present calculations, but have not yet been verified experimentally. Similarly, the $L_1\ ^2\Phi_{7/2}$ and $L_2\ ^2\Phi_{5/2}$ states found in the present work have also not yet been observed.

I. INTRODUCTION

With the introduction of relativistic effective core potentials (RECPs) which include the spin–orbit interaction,[1–3] it has become feasible to carry out accurate configuration interaction (CI) studies of the electronic spectra of molecules containing heavy atoms such as lead and bismuth. Recent examples of this type of investigation in our own laboratory have been reported for the BiF (Ref. 4) and BiH (Ref. 5) diatomic systems, e.g., and the results have been found to be in generally good agreement with relevant experimental data in each case, both for energy-related properties and also for details of intensity distributions and radiative lifetimes of excited electronic states. The oxide of bismuth is an obvious candidate for additional calculations, especially since it is an odd-electron system unlike the first two diatomic species mentioned. It is isovalent with the NO molecule and is well-known[6] to possess a $^2\Pi$ ground state with a very large separation between the $\Omega=1/2$ and 3/2 components.

From a technical point of view, there is a key difference between even- and odd-electron systems when treated with standard configuration interaction CI techniques in which only Abelian spatial groups such as C_{2v} or D_{2h} are given explicit consideration in analyzing the many-particle electronic wave functions which form the basis for such calculations. In C_{2v} symmetry, there are four distinct double group irreducible representations for systems with an even number of electrons into which the various electronic configurations can be divided in order to reduce the sizes of secular equations which need to be solved directly in a given application, but for odd-electron systems such as BiO, no such simplification is possible. This state of affairs therefore leads to additional complications when the relativistic effects of a molecule such as BiO are considered as compared to those of their even-electron counterparts.

Spectroscopic investigations of bismuth oxide date back to the work of Mecke and Guillery[7] in 1927. Until recently, only four excited valence electronic states had been reported,[6,8] denoted as $A\ ^2\Pi_{1/2}$, $B\ ^4\Sigma^-_{1/2}$, $C\ ^2\Delta_{3/2}$, and $D\ ^2\Pi_{1/2}$. In addition several higher-lying states of Rydberg type have been reported which are not as well characterized as the $A-D$ states. Based on the above assignments, a number of other excited states are clearly expected, such as the $\Omega=3/2$ counterparts of the $X_1\ ^2\Pi_{1/2}$ ground and the $A\ ^2\Pi_{1/2}$ excited states, but no direct experimental evidence for these species has been found. This prompted Shestakov *et al.*[9] to reinvestigate this molecular spectrum by means of chemiluminescence experiments. By employing a high-resolution Fourier-transform spectrometer, these authors were able to identify four new electronic states and ten new transitions. This work was carried out during the same period when the present relativistic CI calculations were under way, and so in a number of cases, it was possible to test the predictions of the theoretical study, both with regard to the energy locations of transitions as well as their absolute intensities. The results of these calculations are reported below and it will be seen that numerous comparisons with available experimental data are possible on this basis.

[a]Fellow of the Alexander von Humboldt Foundation; on leave from the Institute of Physics, St. Petersburg State University, St. Petersburg, Russia.

 0021-9606/94/100(12)/8956/13/$6.00

II. DETAILS OF THE THEORETICAL TREATMENT

The semicore RECP of Christiansen[10] has been employed to describe the bismuth inner-shell electrons. The same potential gives good results for the BiF molecule,[4] although it leads to overestimations in the 0.05–0.10 Å range for the equilibrium bond lengths of the various electronic states. In this treatment, only the $5d$, $6s$, and $6p$ valence electrons of bismuth are described via basis functions. At the self-consistent field, (SCF) stage of the calculations, the averaged (spin-independent) RECPs are employed, whereas the spin–orbit potentials are introduced at the correlated level of the present theoretical treatment. The atomic orbital (AO) basis employed for bismuth is adapted from the Cartesian Gaussian set recommended by Ross *et al.*[11] It consists of a $(3s,3p,4d)$ primitive set in which a (2,1,1) contraction is employed for the d functions. The oxygen basis is taken from Ref. 12 and consists of four s and four p primitives, augmented by a single d function with an optimized exponent of $1.33a_0^{-2}$. It is used in conjunction with a RECP from the same reference to describe the oxygen $1s$ electrons.

The configuration interaction calculations are carried out on the basis of the SCF MOs of the BiO^+ ion with its closed-shell ground electronic configuration. Although the treatment only takes explicit consideration of the symmetry elements of the C_{2v} point group, it nonetheless produces MOs which transform according to the full linear point group. The use of an ionic configuration has the advantage of allowing the virtual orbitals to be computed in the field of less than the full complement of BiO electrons, thereby rendering them quite suitable for describing correlation effects at the next stage of the calculations, as has been demonstrated earlier in tests for the NO_2 molecule.[13] For this purpose, 20 valence electrons are treated explicitly, including those of the $5d$ subshell of the bismuth atom.

The CI calculations are carried out in two stages. At first, only the averaged RECPs are considered in order to produce a series of λ–s electronic wave functions, i.e., eigenfunctions of the S^2 operator as well as of the orbital angular momentum component along the internuclear axis. For this purpose, only 11 electrons are included in the active space, with the five MOs corresponding to the $5d$ bismuth subshell employed as a fixed core in all configurations. The standard multireference single- and double-excitation CI method is employed (MRD-CI),[14] with configuration selection and perturbative energy extrapolation. The calculations are carried out with the Table CI algorithm[15] for efficient handling of the various open-shell cases. A selection threshold of $T=1.5\times10^{-5}E_h$ is employed throughout. Information about sizes of reference spaces and the corresponding generated and selected secular equations and the numbers of roots treated are given in Table I, as well as the values of the sums of squares of coefficients for all reference configurations for a number of low-lying states of each symmetry. Results are obtained for a range of internuclear distances from $r=3.3$ to $5.0a_0$ in steps of $0.1a_0$, as well as for selected points for larger separations. The importance of higher excitations in the CI treatment has been assessed by applying the generalized multireference analog of the Davidson correction[16,17] to the extrapolated $T=0$ energies of each root. In addition, electric dipole matrix elements have been calculated for all pairs of states for which these quantities do not vanish because of symmetry. For this purpose, only the variational wave functions are employed, however.

TABLE I. Technical details of the MRD-CI calculations.[a]

C_{2v} symmetry	$N_{\text{ref}}/N_{\text{root}}$	SAFTOT/SAFSEL	$C_{\infty v}$ notation	Σc_p^2
$^2B_{1,2}$	72/6	1 662 031/8476	$1\,^2\Pi$	0.9334
			$2\,^2\Pi$	0.9377
			$1\,^2\Phi$	0.9401
$^2A_1$	77/5	1 666 172/7973	$1\,^2\Sigma^+$	0.9216
			$1\,^2\Delta$	0.9252
$^2A_2$	65/5	1 626 295/6435	$1\,^2\Sigma^-$	0.9293
			$1\,^2\Delta$	0.9247
$^4B_{1,2}$	49/3	1 410 499/7478	$1\,^4\Pi$	0.9387
			$2\,^4\Pi$	0.9101
$^4A_1$	50/3	1 396 695/5805	$1\,^4\Sigma^+$	0.9236
			$1\,^4\Delta$	0.9274
$^4A_2$	64/3	1 475 910/5651	$1\,^4\Sigma^-$	0.9272
			$1\,^4\Delta$	0.9286
$^6A_1$	53/2	1 456 927/5066	$1\,^6\Sigma^+$	0.9115
$^6B_{1,2}$	13/1	414 327/2374	$1\,^6\Pi$	0.9204

[a]The number of selected SAFs and the Σc_p^2 values (for the lowest roots of each symmetry) are given for $r=3.8a_0$. SAFTOT designates the total number of SAFs generated. SAFSEL is the number of selected SAFs, N_{ref} and N_{root} refer to the number of reference configurations and roots treated, respectively.

The final step in the theoretical treatment is to carry out a relativistic CI in which the spin–orbit interaction is included via the RECPs. The λ–s eigenfunctions described above are associated with appropriate spin functions (different M_s values) in order to define a basis for the final secular equations. For doublet states of A_1 and A_2 (Σ^+, Σ^-, and Δ) symmetries, $M_s=-1/2$ components are employed, while for $^2B_1$ and $^2B_2$ states, the $M_s=1/2$ counterparts are taken. For quartets, components with $M_s=1/2$ and $-3/2$ are added for the B_1 and B_2 species, and $M_s=3/2$ and $-1/2$ for those of A_1 and A_2 symmetry. As mentioned in the Introduction, states of all four C_{2v} spatial symmetries need to be mixed in the same secular equation for such an odd-electron system. A completely equivalent secular equation is also solved for the complementary set of M_s values which gives identical CI energies, but orthogonal eigenfunctions to those of the first set. The latter results are needed in order to compute dipole moment matrix elements for perpendicular transitions. The present procedure is less time consuming than the alternative method of simply mixing all selected configuration state functions (CSFs) for each λ–s space and diagonalizing, such as has been done, e.g., in the previous calculations for BiF (Ref. 4) and BiH (Ref. 5). Explicit tests have shown that the present technique of introducing the spin–orbit interaction gives results of comparable accuracy, even though relatively small secular equations are involved in the final step.

Once the electronic CI data are at hand, the potential surfaces are fitted to polynomials for use in the corresponding nuclear motion Schrödinger equations, and these are solved numerically by means of the Numerov–Cooley method.[18] The electronic dipole transition matrix elements are computed by summing over results for pairs of λ–s states with identical spin functions, and the results are also

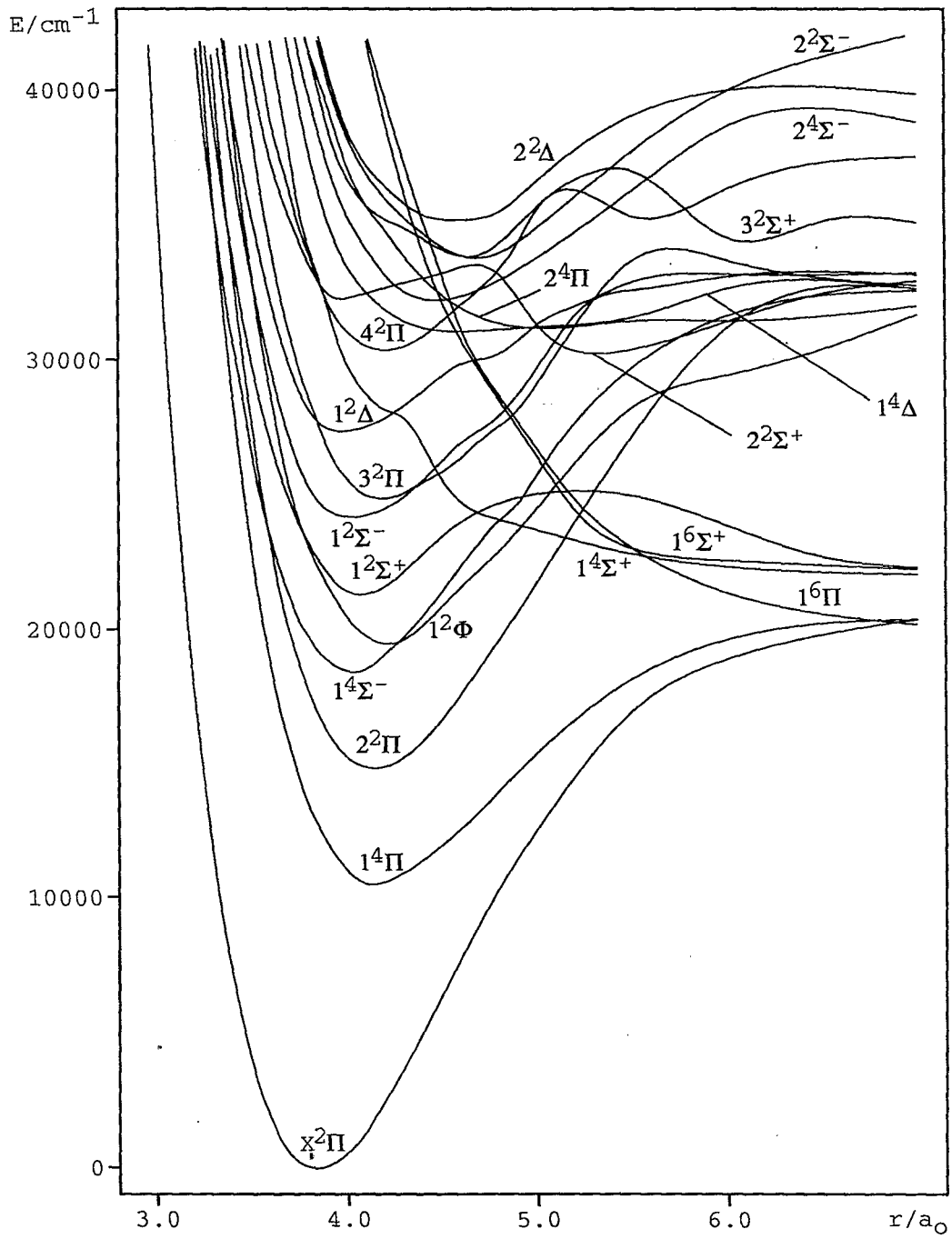

FIG. 1. Computed potential energy curves of the lowest-lying $\lambda-s$ states of the BiO molecule obtained in a theoretical treatment without the inclusion of the spin–orbit interaction.

fitted to polynomials. These data are then averaged over different pairs of vibrational functions to obtain the final electric dipole transition moments, which when combined with the corresponding vibrational transition energies are employed to compute Einstein coefficients for spontaneous emission. The radiative lifetime of a given excited vibrational state is then obtained by summing over the latter quantities for all lower-lying vibrational states and inverting.

III. COMPUTED POTENTIAL CURVES AND VIBRATIONAL ENERGIES

A. Survey of $\lambda-s$ potential curves

The potential curves obtained for bismuth oxide in the CI treatment which neglects the spin–orbit coupling interaction are shown in Fig. 1. The ground state has $^2\Pi$ symmetry with a predominantly $\sigma^2\pi^4\pi^*$ electronic configuration. Both

the π and σ MOs are localized mainly on the oxygen atom, as one would expect on the basis of the relative electronegativities of the two constituents. The π^* (and σ^*) orbitals have a complementary composition, and this fact is important in determining the spin–orbit splitting of the $X\ ^2\Pi$ state, as well as the corresponding results for the various excited states.

The $\pi\rightarrow\pi^*$ excitation produces the lowest-lying excited states of this molecule, beginning with the $^4\Pi$ species. Because of the increase in antibonding character caused by the transition, it is not surprising that the equilibrium bond length of the $^4\Pi$ state is larger than that of $X\ ^2\Pi$. The isovalent NO molecule also possesses a $^4\Pi$ excited state immediately above its $X\ ^2\Pi$ ground state, so this result is hardly surprising. Nonetheless, it is interesting that previous assignments of the observed transitions in the BiO spectrum[6,8,19] have made no mention of such a low-lying quartet state. The same $\sigma^2\pi^3\pi^{*2}$ configuration leads to three $^2\Pi$ states and one of $^2\Phi$ symmetry, and their potential curves are also found in Fig. 1. The corresponding equilibrium bond distances are all quite similar to that of $^4\Pi$.

The other competing electronic configurations which produce relatively low-lying BiO excited states are produced by $\pi^*\rightarrow\sigma^*$ and $\sigma\rightarrow\pi^*$ excitations. The first of these leads to a lone $^2\Sigma^+$ state, whose analog in the NO molecule is the well-known A species. The other produces $^{4,2}\Sigma^-$ and $^2\Delta$ states and another higher-lying $^2\Sigma^+$ species. All these states possess bond distances which are close to those of the $\pi\rightarrow\pi^*$ excited states discussed first, and thus do not produce of themselves any avoided crossings. Near the $X\ ^2\Pi$ r_e value, the next lowest-energy configuration comes from the $\pi\rightarrow\sigma^*$ excitation. This leads to two $^2\Sigma^+$, $^2\Sigma^-$, and $^2\Delta$ states each and one quartet state of each of these Λ values as well. The potential minima for this series of states occur at somewhat larger bond distances than for the $\pi\rightarrow\pi^*$, $\sigma\rightarrow\pi^*$, and $\pi^*\rightarrow\sigma^*$ states already discussed.

Finally, there are a number of repulsive potential curves resulting from double excitations out of bonding orbitals. Two of them belong to the $^6\Pi$ and $^6\Sigma^+$ states which correlate with the Bi (^4S_u)+O (^3P_g) dissociation limit (corresponding to the atomic ground state in each case). It is obvious from the multiplicities of the latter two atomic states that any molecular configuration correlating with it must have five open shells and this situation is reached by adding one electron each to the π^* and σ^* MOs relative to the ground state configuration. From Fig. 1, it can be seen that the $^4\Sigma^+$ state of the same configuration as $^6\Sigma^+$ interacts strongly with the $\pi\rightarrow\sigma^*$ state of the same symmetry in the neighborhood of $r\approx 4.4a_0$. The resulting lowest-lying $^4\Sigma^+$ state will be seen to lead to a number of important avoided crossings once the spin–orbit interaction is included in the theoretical treatment. This $\lambda-s$ state and corresponding five-open-shell $^{4,2}\Pi$ and $^2\Sigma^+$ states also correlate with the lowest dissociation limit. The latter state also causes some interesting avoided crossings in the same, general bond length region as $^4\Sigma^+$ (Fig. 1).

B. Relativistic CI energy results

The lowest-energy $\lambda-s$ states have then been taken as basis functions for a further CI treatment in which the spin–orbit interaction has been included via the RECPs. Five states each of $^2B_1$, $^2B_2$ (four $^2\Pi$ and one $^2\Phi$), and $^2A_1$ (three $^2\Sigma^+$ and two $^2\Delta$) states have been chosen, along with four of $^2A_2$ type (two $^2\Sigma^-$ and the other components of the two $^2\Delta$ states). Among the quartet states, two each of B_1, B_2 ($^4\Pi$), and A_1 ($^4\Sigma^+$ and $^4\Delta$) are included, plus three of A_2 symmetry (two $^4\Sigma^-$ and one $^4\Delta$). In a given secular equation, each of the quartet functions is included with two different M_s values (see Sec. II), so the order of the resulting relativistic CI secular equation is 37×37. Sextet $\lambda-s$ states have not been included, but they are not expected to play a significant role in describing the BiO spectrum.

The resulting potential energy curves are shown in Fig. 2. As expected from the $\lambda-s$ results, it is found that the (X_1) ground state is predominantly $^2\Pi_{1/2}$, at least up to $r=4.5a_0$. Coefficients for the various $\lambda-s$ basis functions in the final spin-perturbed CI eigenvectors are shown in Table II for the $\Omega=1/2$ states and in Table III for those with $\Omega=3/2$. The $\Omega=1/2$ state is lower by virtue of the fact that the corresponding open-shell π^* MO is only singly occupied (regular order). The T_e value for the $X_2\ ^2\Pi_{3/2}$ excited state is computed to be 6809 cm^{-1}, or 280 cm^{-1} smaller than the corresponding experimental value.[9] Results for T_e values, equilibrium bond lengths, and vibrational frequencies are given in Table IV. The bond length of $X_1\ ^2\Pi_{1/2}$ is computed to be 2.046 Å, which is 0.112 Å larger than measured. Such an error is consistent with our experience in calculations for the BiF spectrum,[4] although in that case, the overestimation is somewhat smaller (0.06 Å for the 0^+ ground state). It is clear from results for the latter system[4] that one cause for these discrepancies lies in the choice of the RECP employed for the bismuth atom,[10] but additional tests for BiO show that significantly better bond distance results are obtained with the same core potentials by incorporating d-shell correlation effects in the theoretical treatment. Errors of similar magnitude and direction are expected for BiO excited states, however, and so the relationship between the various potential curves in Fig. 2 are still expected to parallel quite closely those for the exact results, and thus the computed Franck–Condon factors should still be of high accuracy. The calculated frequency is too low by 44 cm^{-1} (Table IV), consistent with the overestimation of the bond distance. For $X_2\ ^2\Pi_{3/2}$, there is an indication of a slightly smaller bond length and frequency. No value for the $X_2\ ^2\Pi_{3/2}$ bond distance is as yet known from experiment, but the frequency has been measured[9] to be 4 cm^{-1} lower than for the $\Omega=1/2$ state.

The shapes of the lowest two potential curves (Fig. 2) are quite similar at relatively small r values, but an avoided crossing between the upper curve and that of a second $\Omega=3/2$ state (A_1) changes this picture drastically at larger separations (Fig. 2). Experimentally, perturbations in the regular vibrational structure of the $X_2\ ^2\Pi_{3/2}$ state have been found[9] for $v>6$, which was the first indication of a second $\Omega=3/2$ species expected to lie below the well-known $A\ ^4\Pi_{1/2}$ (hereafter referred to as A_2) state with a T_e value of 14 195 cm^{-1}. We will consider this avoided crossing in more

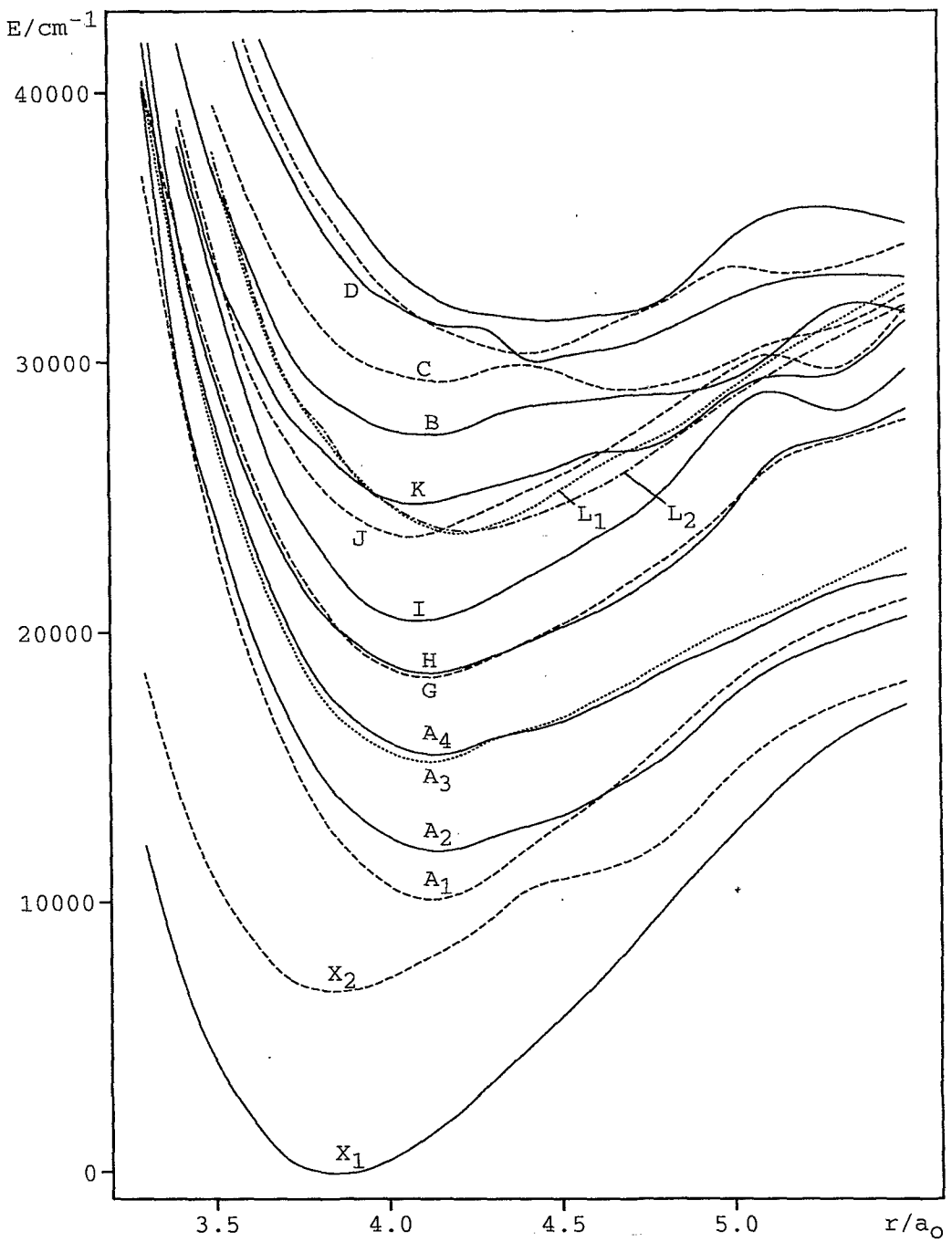

FIG. 2. Computed potential energy curves for the lowest-lying electronic states of the BiO molecule in the present theoretical treatment including spin–orbit coupling (solid curves for $\Omega=1/2$ states, dashed curves for $\Omega=3/2$, dotted curves for $\Omega=5/2$, and a dotted–dashed curve for $\Omega=7/2$).

detail in Sec. III C, but at this juncture, it should be noted from Table II and III that the composition of the A_1 and A_2 states is not mainly $^2\Pi$, as originally assumed,[19] but rather $^4\Pi$. This result must be anticipated based on the $\lambda-s$ potential curves of Fig. 1, but presumably was not given serious consideration previously because of the belief that the well-known A_2-X_1 band system is too strong to result from a $^4\Pi-^2\Pi$ transition. A significant admixture of $2\,^2\Pi$ and $3\,^2\Pi$ character is also found to be present in the $A_1\,^4\Pi_{3/2}$ wave function which helps to overcome this objection, however, as will be discussed in Sec. IV, when the results of the transition probability calculations are considered. Since both the $X\,^2\Pi$ and $A\,^4\Pi$ $\lambda-s$ states converge to the same dissociation limit, it is clear that the energy splitting between them must gradually decrease with increasing internuclear separation. This fact is clearly consistent with the observation of significant perturbations in the vibrational level pattern for the $X_2\,^2\Pi_{3/2}$ state, as discussed above.

TABLE II. The composition of the nine lowest $\Omega=1/2$ states of BiO [$c^2(\%)$] at various bond distances r (in a_0).[a]

State	r	$1\,^2\Pi$	$2\,^2\Pi$	$3\,^2\Pi$	$4\,^2\Pi$	$1\,^2\Sigma^+$	$2\,^2\Sigma^+$	$1\,^2\Sigma^-$	$2\,^2\Sigma^-$	$1\,^4\Pi$	$2\,^4\Pi$	$1\,^4\Sigma^-$	$2\,^4\Sigma^-$	$1\,^4\Sigma^+$	$1\,^4\Delta$
$X_1\,^2\Pi_{1/2}$	3.3	96.1										1.0			
	3.8	91.9				1.2	1.2			1.9		1.3			
	4.1	87.5		2.6		1.8	1.4			3.5		1.5			
	4.5	76.4		5.4		1.9	2.1			7.5		2.0			1.9
	5.0	66.5	1.0	11.0		2.4	1.5			10.7		1.4			2.8
	5.5	53.7			14.7					19.6					5.5
$A_2\,^4\Pi_{1/2}$	3.3			3.9			9.4	2.5		31.4		47.6			
	3.5			7.1	2.7		4.7	1.8		62.7		17.1			
	3.8	1.0		8.1	3.0		2.8	1.2		71.0		7.6			
	4.1	3.0		8.2	3.6		2.2	1.0		70.7		4.8		1.0	2.0
	4.5	7.1		5.7	4.9		3.4	1.2		65.2		5.3	1.7	1.2	2.2
	5.0	14.9		5.0			2.8			70.6		1.2	1.4	1.3	1.0
	5.5	26.4			3.0		2.0		1.1	60.9					
$A_4\,^4\Pi_{1/2}$	3.3	1.4	2.6	3.2			1.2	1.7		67.2		21.4			
	3.5		1.2				1.3			80.3		13.9			
	3.8									92.7		3.8		1.0	
	4.1									93.2		2.3		1.4	
	4.5	1.8								92.3		1.4		1.6	
	5.0	2.7	1.6							88.8		1.0		2.5	
	5.5	1.8							4.0	86.9				1.5	
$H\,^2\Pi_{1/2}$	3.3		2.0				3.6	7.8		75.6		8.3			
	3.5	2.3	6.7				8.9	4.2		35.3		39.7			
	3.8	2.9	20.5		2.2		10.2	3.8		13.8		43.2			
	4.1	2.0	47.7		3.0		6.2	2.4		7.4		25.7			
	4.5	5.7	35.9		4.0		7.4	2.9	1.0	10.3	4.8	26.7			
	5.0	1.8	69.7			2.7	2.4		2.3	5.2	1.9	8.6		2.0	
	5.5		3.2						1.5					92.1	
$I\,^4\Sigma^-_{1/2}$	3.3		2.0			94.0					3.0		1.0		
	3.5		83.2	7.8								4.7			
	3.8		69.1	7.4			3.1					13.6			
	4.1	3.1	41.4	5.6			7.2	2.4		1.6	3.0	31.9			
	4.5	2.7	52.2	5.8			5.3	1.6			5.2	22.4			
	5.0	2.0	7.6	2.0		13.0	3.3				3.0	56.4		2.9	
	5.5	2.1	15.4			68.2			1.1	4.4	1.3	2.9		3.3	
$K\,^2\Sigma^+_{1/2}$	3.3		85.0	7.7				1.0				3.0			
	3.5				1.2	91.1					4.2		1.6		
	3.8				3.1	85.0		2.1			5.2		2.8		
	4.1	1.4			4.4	79.6		2.4			6.9		4.0		
	4.5	1.4			5.7	68.9		3.8			12.7		6.1		
	5.5	1.4	18.4	34.5	1.0	8.5				2.8	1.0				27.0
$B\,^2\Sigma^-_{1/2}$	3.3		2.1				6.7	71.2		10.1		7.9			
	3.5				2.0		5.5	74.8		3.5		11.8			
	3.8				3.2	2.7	4.0	69.7		1.0	2.5	14.9			
	4.1				6.9	3.3	2.6	61.1			4.8	17.0			
	4.5				7.3	2.5	1.4	46.5	1.8	1.8	13.7	18.2		4.1	
	5.0	1.6	8.3			12.8			3.0	2.6	3.1	2.3	7.9	53.8	
	5.5		42.3			13.5			1.6	2.1	2.0	1.5	8.9		8.0
$D\,^2\Pi_{1/2}$	3.3		2.0	20.0	27.8		27.8	10.1		4.6		5.4			1.5
	3.5		1.2	4.0	74.9			6.0		3.7		1.6			5.3
	3.8		1.1	1.8	63.2	1.2		7.5		4.4			1.6	1.7	15.1
	4.1				46.5	1.0	1.0	10.1		3.5	2.5		3.4	1.7	29.0
	4.5			1.0	10.5	1.0			6.7				6.5	26.6	37.5
	5.0	2.7		9.1	1.0						10.3				73.3
	5.5		6.2	1.3		2.0					15.0	4.0	39.1		17.4
$\Omega=1/2$	3.3			9.1	64.5		21.0								1.5
	3.5		3.9	56.5	10.9		16.0	2.0		6.1	1.0	1.2	1.5		
	3.8		3.1	48.4	7.8		3.1		2.4	8.7	3.6		5.6	15.4	
	4.1			3.3				2.4	10.4	3.6	4.4		4.1	68.6	1.6
	4.5	1.7		2.2	4.6			13.6	7.7	9.2				30.8	26.9
	5.0				1.2	1.4		77.6			15.3				
	5.5		3.1				30.6	2.9			38.5	2.0	18.5		

[a]The most important configurations and some of the resulting $\lambda-s$ states are $\sigma^2\pi^4\pi^*$ ($^2\Pi$); $\sigma^2\pi^3\pi^{*2}$ ($^2\Pi,^4\Pi$); $\sigma^2\pi^4\sigma^*$ ($^2\Sigma^+$); $\sigma\pi^4\pi^{*2}$ ($^2\Sigma^+,^2\Sigma^-,^2\Delta,^4\Sigma^-$); $\sigma^2\pi^3\pi^*\sigma^*$ ($^2\Sigma^-,^2\Delta,^4\Sigma^+,^4\Delta,^4\Sigma^-$); and $\sigma\pi^4\pi^*\sigma^*$ ($^4\Pi$). Entries are only made for contributions with $c^2\geq 1.0\%$.

TABLE III. The composition of the six lowest $\Omega=3/2$ states of BiO [$c^2(\%)$] at various bond distances r (in a_0).[a]

State	r	$1\,^2\Pi$	$2\,^2\Pi$	$3\,^2\Pi$	$4\,^2\Pi$	$1\,^4\Pi$	$2\,^4\Pi$	$1\,^4\Sigma^-$	$2\,^4\Sigma^-$	$1\,^4\Sigma^+$	$1\,^2\Delta$	$2\,^2\Delta$	$1\,^4\Delta$
$X_2\,^2\Pi_{3/2}$	3.3	94.6						2.9			1.5		
	3.8	92.2				1.0		3.5			1.9		
	4.1	90.6		2.0				3.6			1.9		
	4.3	71.2	4.2	9.5		7.4		2.1	1.6		1.1	1.9	
	4.5	29.9	8.4	16.8	1.5	35.0			2.5	2.4		1.6	1.2
	5.0	40.1	1.9	17.2		32.8			2.4	2.6		1.4	1.3
	5.5	39.2		1.2	16.6	34.9			1.8	1.4		1.3	2.2
$A_1\,^4\Pi_{3/2}$	3.3		12.9	12.6		70.5		2.0					
	3.8		15.3	14.7		64.6				1.9			
	4.1		13.7	14.8		64.3			1.2	2.7			1.9
	4.3	18.0	8.4	8.0		56.4		1.6		2.9			2.3
	4.5	57.6	1.4			31.7		3.0		1.1	1.9		1.5
	5.0	49.4		1.3		42.0		1.0		1.1		2.1	1.7
	5.5	38.8				51.5						4.9	1.8
$G\,^2\Pi_{3/2}$	3.3	1.4	12.1	1.1		22.6		60.4					
	3.5		36.3		1.2	7.3		52.1					
	3.8		59.4			7.9		21.5		1.0			
	4.1		67.0			15.7		12.0		1.6			
	4.5		62.4			13.5		17.1		3.7			
	5.0		64.7			5.7		13.7		13.1			
	5.5		5.7			2.7			1.7	89.1			
$J\,^4\Sigma^-_{3/2}$	3.3	1.2	62.9			14.4		13.9			5.3		
	3.5	2.0	44.0	1.1	1.9	9.2		39.5					
	3.8	2.6	19.5	3.3	3.6	2.1		66.8					
	4.1	2.1	12.1	6.3	5.2		1.3	70.2	1.0				
	4.5	1.0	16.9	11.0	4.8		2.2	55.7	1.6	1.2			
	5.0		1.2	2.9				21.3	5.2	60.5			1.8
	5.5		69.5					9.5	4.0	5.0	3.2		2.6
$C\,^2\Delta_{3/2}$	3.3		4.1	3.9	3.3	2.5					78.4		
	3.5			8.8	6.8	2.2	1.0	1.0			77.9		
	3.8			16.2	8.2	3.6	1.9	2.6	1.0		65.8		
	4.1			26.4	7.6	6.6	2.9	6.4	2.7		45.9		
	4.5			19.6	4.1	7.0	7.7	7.2	4.9	1.0	46.8		
	5.0		20.0	10.8		5.9	1.9	35.9	6.4	4.7			
$\Omega=3/2$	3.3	1.5	3.1	76.1	1.0	9.9			1.4		5.7		
	3.5	2.4	3.0	67.5		10.1		1.0	2.9		11.6		
	3.8	2.9	3.4	37.8		10.3		1.0	11.9	15.0	15.4		
	4.1		1.1		1.5	1.2	6.5		8.3	20.8	57.1		
	4.5		2.2		1.5	2.2			24.1	55.8	5.0	1.6	5.4
	5.0	1.5		1.6		3.3	5.0	10.0			11.5	11.6	55.1
	5.5							43.0			11.7		35.8

[a]The same footnote as in Table II.

The A_2 state with $\Omega=1/2$ also turns out to have a dominant $^4\Pi$ contribution (Table II), but does not contain such a large admixture of $^2\Pi$ $\lambda-s$ states as the lower-energy $\Omega=3/2$ counterpart. Instead, there is a fairly large contribution from the lowest $^4\Sigma^-$ state, especially for $r<4.0a_0$. The fact that the $^4\Pi_{1/2}$ component lies above $^4\Pi_{3/2}$ is understandable from its $\pi^3\pi^{*2}$ $\lambda-s$ configuration, although the situation is not as clear as for the $X\,^2\Pi$ state since there are now two open-shell π MOs, only one of which (π^*) can lead to large spin–orbit splittings. Even at the equilibrium r value, this energy separation is only 2365 cm^{-1} (Table IV). Moreover, the calculations find that the A_2 potential curve actually crosses that of A_1 (Fig. 2). The computed r_e value for the $A_2\,^4\Pi_{1/2}$ state is 0.0655 Å greater than found experimentally, while the vibrational frequency is only 7 cm^{-1} smaller than measured.[9] There is no experimental value for the $A_1\,^4\Pi_{3/2}$ bond distance, but it is computed to be 0.02 Å smaller than that of $A_2\,^4\Pi_{1/2}$. The vibrational frequency is overestimated in this case, as will be discussed in more detail in Sec. III C, and this seems to be a direct consequence of the nonadiabatic effects associated with the avoided crossing between the lowest two $\Omega=3/2$ states of this molecule. The T_e value of the $A_2\,^4\Pi_{1/2}$ state is underestimated in the present calculations by 1937 cm^{-1}, while the energy splitting relative to A_1 is too small by 760 cm^{-1} (Table IV), i.e., the T_e value for the latter is in somewhat better agreement with experiment.

Because of the importance of the $^4\Pi$ $\lambda-s$ species in the composition of the A_1 and A_2 states, it must be expected that two other states be found in the same energy range with $\Omega=5/2$ and 1/2, respectively. The results of Fig. 2 show that two such states are present with T_e values (Table IV) of 15 445 cm^{-1} ($A_3\,^4\Pi_{5/2}$) and 15 760 cm^{-1} ($A_4\,^4\Pi_{1/2}$). Examination of the corresponding eigenfunctions indicates that the $M_s=3/2$ $\lambda-s$ component of the $^4\Pi$ is involved in this case, whereas the corresponding $M_s=1/2$ components

TABLE IV. Calculated and experimental spectroscopic properties of BiO (transition energies T_e, bond lengths r_e, and vibrational frequencies ω_e).

State	T_e (cm^{-1})		r_e (Å)		ω_e (cm^{-1})	
	Calc.	Expt.[a]	Calc.	Expt.[a]	Calc.	Expt.[b]
$X_1\ ^2\Pi_{1/2}$	0	0	2.0464	1.934	648	692 (692)
$X_2\ ^2\Pi_{3/2}$	6809	7089	2.0425		634	688
$A_f\ ^4\Pi_{3/2}$	10 653	11 830	2.1864		599	550
$A_2\ ^4\Pi_{1/2}$	12 258	14 195	2.2081	2.1426	498	505 (509)
$A_3\ ^4\Pi_{5/2}$	15 445		2.1931		528	
$A_4\ ^4\Pi_{1/2}$	15 760		2.2088		497	
$G\ ^2\Pi_{3/2}$	18 688	20 178	2.1912		562	502
$H\ ^2\Pi_{1/2}$	18 874	20 470	2.2005		481	472 (472)
$I\ ^4\Sigma^-_{1/2}$	20 848	21 983	2.1810		536	507
$J\ ^4\Sigma^-_{3/2}$	23 983	25 599	2.1588		507	490
$L_f\ ^2\Phi_{5/2}$	24 045		2.2261		541	
$L_2\ ^2\Phi_{7/2}$	24 045		2.2413		477	
$K\ ^2\Sigma^+_{1/2}$	25 205	26 753	2.1772		449	420
$B\ ^2\Sigma^-_{1/2}$	27 784	28 740	2.1892	2.09	479	483 (483)
$C\ ^2\Delta_{3/2}$	29 465	30 210	2.1932	2.1102	451	492 (465)

[a]Reference 6.
[b]Reference 9 (values in parentheses are from Ref. 6).

dominate in the lower-lying A_1 and A_2 states. There is as yet no experimental evidence for either of these states. We will see in Sec. IV that their radiative lifetimes appear to be relatively long, which is undoubtedly the main reason why such low-lying states have not yet been observed. Not surprisingly, the r_e values for this pair of $^4\Pi$-related states are very similar to those computed for the A_1 and A_2 states, particularly the latter (Table IV).

The next states which have been detected experimentally are denoted $G\ ^2\Pi_{3/2}$ and $H\ ^2\Pi_{1/2}$, respectively.[9] The results of Tables II and III show that both of these states derive primarily from the lowest $^2\Pi$ $\lambda-s$ state of the same $\sigma^2\pi^3\pi^{*2}$ electronic configuration which produces the $A\ ^4\Pi$ species. The computed T_e values (Table IV) are each approximately 1500 cm^{-1} smaller than observed.[9] The corresponding energy splitting is computed to be quite small (186 cm^{-1}), as is verified in the measured data ($\Delta E=292$ cm^{-1}). The calculated bond lengths for these two states both fall in the 2.19–2.20 Å range, which has been found for the A states. The $H\ ^2\Pi_{1/2}$ vibrational frequency is measured to be 30 cm^{-1} smaller than for $G\ ^2\Pi_{3/2}$. The calculations find the same order, but are less accurate for the $\Omega=3/2$ state (Table IV). Since a similar situation exists for the A_1-A_2 pair of states, it appears that the avoided crossing affecting the $X_2\ ^2\Pi_{3/2}$ and $A_1\ ^4\Pi_{3/2}$ states of lower energy continues to influence at least the next $\Omega=3/2$ species above them as well. Despite the dominance of the $2\ ^2\Pi$ $\lambda-s$ state in the G and H wave functions in the region of their respective equilibrium distances, it is clear from Tables II and III that important contributions from both the $\pi\rightarrow\pi^*\ ^4\Pi$ and the $\sigma\rightarrow\pi^*\ ^4\Sigma^-$ $\lambda-s$ states are also present, especially at relatively small r values. In addition, the influence of the $^4\Sigma^+$ $\lambda-s$ state which is derived from the $\pi\rightarrow\sigma^*$ configuration (see Sec. III A) is evident for both the G and H states through the occurrence of a shoulder near $r=5.2a_0$ (see also Tables II and III at $r=5.5a_0$). The results emphasize that the potential curves of Fig. 2 come about to a large extent because of a series of very strongly avoided crossings, whereby the interaction mainly responsible for these results is spin–orbit coupling. In other words, it would take considerable imagination to explain the observed BiO spectral data based solely on the $\lambda-s$ potential curves of Fig. 1.

The next two most stable states of the BiO system have large contributions from the $\sigma\pi^4\pi^{*2}\ ^4\Sigma^-$ state at most internuclear distances. The $I\ ^4\Sigma^-_{1/2}$ state is computed to have a T_e value of 20 848 cm^{-1}, in good agreement with the observed value of 21 983 cm^{-1}, with the theoretical value again being too low. Its bond distance is found to be 0.01–0.02 Å smaller than the average calculated value for the various states in which the $\sigma^2\pi^3\pi^{*2}$ configuration dominates, suggesting that the σ MO is slightly less bonding than the π. The $J\ ^4\Sigma^-_{3/2}$ is computed to lie 3135 cm^{-1} higher, in reasonably good agreement with the measured T_e value difference of 3616 cm^{-1}.[9] Its computed r_e value is only 2.1588 Å, over 0.02 Å smaller than that of the I state. The latter's frequency is larger, however, despite this difference in bond distance. Both results are slightly overestimated in the calculations (Table IV). Examination of Table II shows that the designation is actually somewhat arbitrary in the case of the I state, since near its r_e value, it actually has a larger contribution from the $2\ ^2\Pi$ $\lambda-s$ eigenfunction. The H state has previously been denoted as $^2\Pi_{1/2}$, however, referring to the same $2\ ^2\Pi$ function, so it would be somewhat confusing to use the same designation for the I state. A more accurate way to describe these states is in terms of a heavy mixture of the $2\ ^2\Pi_{1/2}$ and $^4\Sigma^-_{1/2}$ $\lambda-s$ eigenfunctions over a large range of r values, whereby significant contributions from $^4\Pi$, $^4\Sigma^+$, $^2\Sigma^+$, $^2\Sigma^-$, and $3\ ^2\Pi$ should also not be overlooked. Near $r=5.0a_0$, potential maxima in both the I and J states occur as a result of the $^2\Sigma^+$ and $^4\Sigma^+$ $\lambda-s$ states' admixture, respectively. Particularly since such relatively small portions of the final wave functions can have a major influence on properties such as transition probabilities, it can be quite misleading to insist on associating each state with a single $\lambda-s$ eigenfunction.

As mentioned in Sec. III A, the $\sigma^2\pi^3\pi^{*2}$ configuration also contains a state of $^2\Phi$ symmetry and the calculations indicate that the corresponding $\Omega=7/2$ and 5/2 species occur in the same energy region as $J\ ^4\Sigma^-_{3/2}$ lying somewhat below the latter for $r>4.2a_0$. Since the theoretical treatment is carried out in formal C_{2v} symmetry, there is some mixing between these nearly degenerate states which complicates the subsequent calculations of transition probabilities to lower-lying states (Sec. IV). There is no experimental evidence for either of the two states in question. According to the electric dipole selection rules, the $\Omega=7/2$ (I_1) state should only have allowed downward transitions to $A_3\ ^4\Pi_{5/2}$, which certainly is the main factor hindering its detection experimentally. The corresponding $^2\Phi_{3/2}$ (L_2) state has dipole-allowed perpendicular transitions to $X_2\ ^2\Pi_{3/2}$, however, so there would seem to be some hope of confirming the present assignment on this basis.

The calculations also indicate another state in this energy region (Fig. 2), namely, $K\ ^2\Sigma^+_{1/2}$, which corresponds to a $\pi^*\rightarrow\sigma^*$ excitation relative to the $X\ ^2\Pi$ ground state. An experimental search for this state was successful,[9] with our computed T_e value again underestimating the observed result

by roughly 1500 cm^{-1} (Table IV). The calculations indicate that its equilibrium bond distance is nearly identical to that of the I state of equal Ω value, but no experimental value has yet been forthcoming. The computed vibrational frequency is found to be overestimated by 29 cm^{-1}.

The next lowest-energy state is computed to be the $B\ ^2\Sigma^-_{1/2}$. Although it has been known from spectroscopic measurements for some time,[6,19] it has previously been assigned to the $^4\Sigma^-$ $\lambda-s$ state. The present calculations indicate (Table II) that a 10%–20% contribution from $^4\Sigma^-$ is present, but by far the largest CI coefficient comes from the doublet of the same $\sigma\pi^4\pi^{*2}$ configuration. The calculated r_e value is too high by 0.10 Å, but this is quite consistent with the results for the ground state (Table IV) and thus serves to further support the correctness of the present assignment. The present ω_e result also fits in quite well with experiment. Near $r=4.5a_0$, its potential curve contains a broad shoulder as a result of an avoided crossing with the $\pi\rightarrow\sigma^*\ ^4\Sigma^+$ state mentioned earlier. This finding is consistent with the fact that only six vibrational levels have been observed for the B electronic state.[19] The next state is $C\ ^2\Delta_{3/2}$, which agrees perfectly with the original assignment.[6,19] It comes from the same configuration as $B\ ^2\Sigma^-_{1/2}$, with a fairly large contribution from the $3\ ^2\Pi$ $\lambda-s$ state as well. The computed T_e value is underestimated by only 745 cm^{-1}, whereas for the B state, the error is 956 cm^{-1}, again in the same direction. The best indication from experiment is that the present computed r_e value is too large by 0.08 Å, while the corresponding ω_e value is too low by either 14 (Refs. 6 and 19) or 41 cm^{-1},[9] again consistent with the errors noted for the same quantities for most of the lower-lying states. In this case, only two vibrational levels have been observed, again probably because of the potential maximum computed for it (Fig. 2) which arises because of the interaction with the $\pi\rightarrow\sigma^*$ $^4\Sigma^+$ and the $\sigma\rightarrow\pi^*\ ^4\Sigma^-$ $\lambda-s$ species.

At this point, the density of states becomes notably greater, with $^2\Delta_{5/2}$, $^2\Pi_{1/2}$, $^4\Delta_{5/2,3/2,1/2}$, and $^4\Sigma^+_{3/2,1/2}$ potential curves lying only slightly above that of $C\ ^2\Delta_{3/2}$. Of these, only the $D\ ^2\Pi_{1/2}$ state is known experimentally. Its T_e value is again underestimated by the present calculations (~1600 cm^{-1}). Consideration of Table II shows that it is the $4\ ^2\Pi$ $\lambda-s$ state which makes the main contribution to $D\ ^2\Pi_{1/2}$, rather than $3\ ^2\Pi$ of the same $\pi\rightarrow\pi^*$ configuration. The present calculations do not actually find a minimum in this state's potential curve for distances less than $4.3a_0$, but rather only a shoulder. A minimum is found at somewhat larger r values (Fig. 2), however, which arises primarily because of an interaction with the $\pi\rightarrow\sigma^*\ ^4\Sigma^+$ and $^4\Delta$ states. Experimentally, only a single vibrational level has been found for the $D\ ^2\Pi_{1/2}$ state, which suggests that there is a very shallow minimum at smaller r values, but at the same time that the deeper minimum caused by the $^4\Sigma^+$ and $^4\Delta$ interactions is simply not observed. There is also a slight possibility that the D state actually corresponds to the next higher $\Omega=1/2$ species, which has a complementary composition to that just discussed. If so, its computed T_e value would be in somewhat better ageement with the experimental result of 32 805 cm^{-1},[6] but in so doing, it would also be somewhat inconsistent with our experience with the other calculated results, which invariably underestimate T_e values by ~1500 cm^{-1}. A number of other low-lying bound electronic states is indicated by the calculations, in addition to those just mentioned in the immediate neighborhood of $D\ ^2\Pi_{1/2}$. Two of them are shown in Fig. 2, but will not be discussed further.

C. Nonadiabatic interaction between the $X_2\ ^2\Pi_{3/2}$ and $A_1\ ^4\Pi_{3/2}$ states

The recent experiments of Shestakov *et al.*[9] find the $\Delta G_{1/2}$ value for the $X_2\ ^2\Pi_{3/2}$ ground state to be 679 cm^{-1}, with a typical anharmonicity characterizing the vibrational progression toward higher energy. There is an abrupt change between $v=6$ and 7, however, with the corresponding ΔG value dropping to 452 cm^{-1} from the previous $\Delta G_{11/2}$ result of 615 cm^{-1}. A glance at Fig. 2 shows what is happening, namely in this energy range there is a rather sharply avoided crossing with the $A_1\ ^4\Pi_{3/2}$ species. Consistent with this conclusion is the observation of the next vibrational level at 12 324 cm^{-1}, only 314 cm^{-1} higher.[9] It is well-known that one has to have a very accurate determination of the energy separation between any two such states in order to describe such nonadiabatic interactions in a suitably quantitative manner. The present calculations fall short of this goal, but the availability of accurate experimental data opens up the possibility of adjusting this quantity in order to extract further information about this interesting effect.

The first step in the theoretical approach employed is to diagonalize the electric dipole operator (z component) in the basis of the X_1 and X_2 adiabatic states. This procedure produces eigenvectors which have quite different dipole moments at each internuclear distance.[20–22] This is because the X_2 dipole moment is much larger ($1.4ea_0$ at the r_e value, with B^+O^- polarity) than its A_1 counterpart, since these two states differ by a $\pi\rightarrow\pi^*$ excitation which produces a charge transfer toward the bismuth atom. By employing these eigenvectors at each r value, one obtains a quasidiabatic basis with which to transform the potential energy. The resulting off-diagonal E_{12} term serves as the coupling matrix element at each internuclear distance which leads to the required nonadiabatic perturbations observed experimentally. A two-state vibrational treatment is then effected,[22] which produces energy levels which can be compared with the measured data.

In the first application of this approach to be considered, the directly computed T_e value (Table IV) is used, and the resulting ΔG values are compared in Table V with their experimental counterparts. There are clear deficiencies in this attempt to describe the observed vibrational structure. The computed dropoff between $\Delta G_{11/2}$ and $\Delta G_{13/2}$ is much less abrupt (469–431 cm^{-1}) than that observed (615–452 cm^{-1}). Moreover, the next level after $v=7$ lies only 5 cm^{-1} higher, instead of the 314 cm^{-1} value observed. The first discrepancy is tied up with the calculated overestimation of the anharmonicity of the X_2 vibrational levels, but the second is caused mainly by the use of the directly computed X_2-A_1 energy separation ΔE.

When the latter quantity is increased, it is found that the best agreement occurs for $\Delta E=+490$ cm^{-1}, at which point, the first vibrational level computed above $v=7$ lies 317

TABLE V. Separation (in cm^{-1}) of successive vibrational levels of the X_2 and A_1 states of BiO. The calculations are done with energy shifts ΔE of 0 and 490 cm^{-1}, respectively; the experimental results are taken from Ref. 9.

v		$\Delta G_{v+1/2}=G(v+1)-G(v)$		
X_2	A_1	Calc. ($\Delta E=0$)	Calc. ($\Delta E=490$ cm^{-1})	Experimental
0		631	632	679
1		618	619	669
2		598	603	659
3		572	583	650
4		529	557	637
5		469	519	615
6		431	474	452
	a	5	317	314
7		410	443	534
	1	607	529	540
8		399	466	521
	2	576	416	530
9				

[a]Separation of the $v=6$ level of X_2 and the $v=0$ level of A_1.

TABLE VI. Radiative lifetimes of excited states of BiO ($v'=0$) calculated partial lifetimes τ_1 and τ_2 for transitions to $X_1\ ^2\Pi_{1/2}$ and $X_2\ ^2\Pi_{3/2}$, respectively, as well as calculated and experimental total lifetimes τ.

	Calculated			Experimental[b]
State	τ_1 (μs)	τ_2 (μs)	τ (μs)	τ (μs)
$X_2\ ^2\Pi_{3/2}$	2700		2700	480
$A_1\ ^4\Pi_{3/2}$	700	1600	500	
$A_2\ ^4\Pi_{1/2}$	10.8		10.8	9.3
$A_3\ ^4\Pi_{5/2}$		6200	6200	
$A_4\ ^4\Pi_{1/2}$	165		165	
$G\ ^2\Pi_{3/2}$	725	14.6	14.3	~15
$H\ ^2\Pi_{1/2}$	8.3		8.3	15
$I\ ^4\Sigma^-_{1/2}$	5.9		5.9	16
$J\ ^4\Sigma^-_{3/2}$	250	25.3	12.6[a]	4.9
$K\ ^2\Sigma^+_{1/2}$	1.0	76	0.96[a]	~2
$B\ ^2\Sigma^-_{1/2}$	1.2	24.1	1.1[a]	0.55
$C\ ^2\Delta_{3/2}$	1.6	1.2	0.68	0.81

[a]Other transitions have been included in the calculation of the total lifetime τ for this state.
[b]Reference 9.

cm^{-1} higher. Furthermore, the next level in the upper-state progression lies 529 cm^{-1} above the latter, compared with a measured $\Delta G_{1/2}$ of 540 cm^{-1}. This shift naturally has very little effect on the lowest vibrational levels of the $X_2\ ^2\Pi_{3/2}$ state (Table V), and thus the computed overstimation of the anharmonicity of this series of energies is still present. Nonetheless, the present calculations suggest that the true diabatic potential curves which are responsible for the observed perturbations in the X_2 vibrational progression must be separated by some 500 cm^{-1} more than computed directly in the present theoretical treatment.

IV. RADIATIVE LIFETIMES OF BiO STATES

The vibrational wave functions of the various BiO electronic states have been combined with electric dipole matrix elements to compute Einstein coefficients for key transitions (Sec. II). The corresponding radiative lifetimes of the $v'=0$ levels of these states are given in Table VI for comparison with available experimental values. The first transition to be considered is between the two components of the $X\ ^2\Pi$ ground state. Shestakov *et al.*[9] have recently measured the $X_2\ ^2\Pi_{3/2}$ radiative lifetime to be 0.48 ms but the present calculations indicate a much longer value of 8.2 ms. Examination of the detailed results indicates that there are a number of small contributions to the electric dipole transition moment at each internuclear distance which tend to cancel one another. It was therefore decided to employ an expanded treatment in which a number of higher-lying $\lambda-s$ states are also included explicitly, leading to 68×68 secular equations at each r value instead of the original 37×37 species (Sec. III B). This procedure does lead to somewhat improved agreement with the X_2 measured lifetime, with the computed value dropping to 2.7 ms (Table VI), but this result still is about five times too large. The transition matrix element decreases with r in the neighborhood of the equilibrium distance, so the fact that the present calculations lead to an overestimate of the latter quantity by 0.10 Å (Table IV) tends to produce corresponding transition probabilities which are too low, and lifetimes that are too long.

In general, it is easily understandable why the transition moment should be relatively small in this case because the result would be zero by symmetry if only $^2\Pi$ contributions to each state were considered. A similar situation exists for the $X_2\ ^3\Sigma^-_1-X_1\ ^3\Sigma^-_0$ transition of BiF, but in this case, good agreement between the computed (1.05 ms) and measured (1.4 ms) lifetime of the upper state is found. A relatively strong admixture of the $^1\Sigma^+$ $\lambda-s$ state in the $X_1\ ^3\Sigma^-_0$ wave function plays an important role in arriving at this result. It also should be mentioned that the spin magnetic dipole moment does not appear to be responsible for the relatively short measured lifetime for $X_2\ ^2\Pi_{3/2}$. A value of 54 ms results on this basis. At the same time, a parallel investigation of the isovalent lead halides[23] yields X_2-X_1 transition probabilities which are in much better agreement with measured values. Thus the origin of the unusually large discrepancy in BiO for the analogous transition is unclear at the present time.

There is as yet no experimental value for the radiative lifetime of the $A_1\ ^4\Pi_{3/2}$ state. It can undergo both parallel and perpendicular transitions to the two electronic states below it. Of these, the $\Delta\Omega=0$ transition to X_2 is weaker, primarily because of the small energy difference (see Sec. III C and Fig. 2). The total lifetime of the $v=0$ A_1 state is computed to be 0.5 ms, while the partial lifetime due to A_1-X_1 transitions is 0.7 ms. Both these values are somewhat longer than the measured X_2 lifetime, but significantly shorter than the corresponding computed value. On this basis, there would seem to be a reasonably good chance of obtaining an experimental value for this quantity in future work. The above results have also been obtained in the expanded relativistic CI treatment. Again lifetime values are two to three times longer if the results of the smaller secular equations are taken. Such distinctions between the two levels of treatment are far more the exception than the rule, however, with most

of the remaining lifetime values to be considered below differing by no more than 10% in the two sets of calculations.

The $A_2(A)^4\Pi_{1/2}-X_1\ ^2\Pi_{1/2}$ parallel transition is fairly strong. In this case, very good agreement is noted between the computed and measured[9] upper-state lifetime, which lies in the 10 μs range (Table VI). As discussed in Sec. III B, the A_2 state is composed primarily of the $^4\Pi$ $\lambda-s$ state with $|M_s|=1/2$. Because A_2-X_1 is such a relatively strong transition, it was natural to assume[6,8,19] that A_2 is predominantly $^2\Pi$ in character, but the results of Table II show that this is not the case. The fact that the $X_1\ ^2\Pi_{1/2}$ ground state has a fairly large $^4\Pi$ component does not seem to explain why the parallel transition moment is still relatively large, but rather $^2\Pi-X\ ^2\Pi$ contributions are primarily responsible. By the same token, since perpendicular transitions between Π states of the same multiplicity are forbidden according to the electric dipole selection rules, it is understandable that transitions to X_2 are quite ineffective in depopulating the A_1 state.

Both the A_1 and A_2 states derive primarily from the $M_s=\pm 1/2$ components of the $\pi\rightarrow\pi^*\ ^4\Pi$ $\lambda-s$ species (Sec. III B). The next two states in the BiO spectrum (A_3 and A_4) are the $\Omega=5/2$ and 1/2 species which arise from the corresponding $M_s=\pm 3/2$ components, however, and they combine only relatively weakly with X_1 and X_2. The computed radiative lifetimes are 6.2 ms ($\Omega=5/2$) and 165 μs ($\Omega=1/2$). This suggests that the latter state can be detected experimentally, although at present, no such results have apparently been reported. Since the computed T_e values of the A_1 and A_2 states underestimate the experimental results by 1200 and 1900 cm^{-1}, respectively, it seems likely that the above undetected states are located at energies which also lie somewhat above those computed (Table IV), probably in the 16 500–17 000 cm^{-1} range. Parallel transitions to X_1 would thus occur in the same energy region where A_2-X_1 $v'\rightarrow 0$ bands are seen with $v'\geqslant 5$. It is especially interesting to see if these predictions are borne out because a positive result would settle the issue of whether the main contributor to the lower A_1 and A_2 excited states is $^4\Pi$ rather than $^2\Pi$ as originally believed.[6,8,19]

The next pair of states (G and H) both have relatively short lifetimes of 15 μs according to recent measurements.[9] The present calculations indicate that the parallel $G-X_2$ transitions are significantly stronger than $G-X_1$. The radiative lifetime of the G state computed on the basis of both transitions is 14.3 μs, in good agreement with the experimental value.[9] There is as yet no indication of whether the parallel transition is the stronger of the two possibilities, however, based on these measurements. The H state also favors parallel transitions, in this case, to $X_1\ ^2\Pi_{1/2}$. Its lifetime is computed to be 8.3 μs on this basis, about one-half of the observed result. This value is also twice as short as that calculated for the G state, whereas the measurements indicate that both states have nearly the same lifetime (Table VI). In general, it seems clear that states which are dominated by $\Lambda=1$ species must prefer parallel transitions between them since perpendicular electric dipole transitions are forbidden between such pairs of $\lambda-s$ electronic states.

The I, J pair of states also have been measured to have relatively short lifetime,[9] with a value of 16 μs reported for I and one of 4.9 μs for J. The present calculations (Table IV) find the opposite ordering, with the J lifetime computed to be 12.6 μs and that of the I state to be 5.9 μs. Parallel transitions are again found to dominate to X_1 in the case of the I state and to X_2 for the J state. The partial lifetime based on the perpendicular $J-X_1$ transition is computed to be much longer (250 μs). The J state lifetime is found to have significant contributions from transitions to six lower-lying states (Table VI).

The agreement between theory and experiment is somewhat better for the determination of the K state's radiative lifetime, with a value of approximately 2 μs having been measured,[9] as compared to the present calculated value of 0.96 μs. The calculations again show that parallel transitions, in this case to $X_1\ ^2\Pi_{1/2}$, are much more probable than perpendicular. The $K-X_1$ transitions are thus the strongest of any in the BiO spectrum considered thus far in the present discussion. In the absence of spin–orbit coupling, only perpendicular transitions are possible between the respective dominant $\lambda-s$ states in the $K-X_1$ transition ($^2\Sigma^+-^2\Pi$), so the finding that the z component of the electric dipole moment is primarily responsible for the computed transition probability again emphasizes the importance of relativistic effects in determining the electronic structure of the BiO system.

In the neighborhood of the J and K states, one finds two other electronic states that derive primarily from the $L^2\Phi$ $\lambda-s$ species, with Ω values of 7/2 and 5/2, respectively. Transitions to X_1 and X_2 are forbidden by the electric dipole selection rules in the former case, whereas perpendicular $5/2\rightarrow 3/2$ transitions are possible in the latter case. The calculations suggest that all of these transitions from the $^2\Phi$-dominated states should be quite weak, and so it is not surprising that no experimental evidence has yet been found for them. Because of symmetry-breaking effects in the calculations caused by the presence of nearly degenerate states of different Ω values, it is very difficult to obtain an accurate value for any of the Einstein coefficients involving the $L\ ^2\Phi$-type excited states, however. Since $^2\Phi$ transitions to both $^2\Pi$ and $^2\Sigma^\pm$ states are spatially forbidden according to the dipole selection rules, it seems unlikely that sufficient intensity is available to allow their experimental detection on the basis of any processes involving lower-energy states.

The next lowest-energy electronic state is the $B\ ^2\Sigma^-_{1/2}$ (Fig. 2), which has previously been assigned as $^4\Sigma^-$.[6,8,19] The observed radiative lifetime[9] is shorter than for any of the lower-lying states discussed above, namely, 0.55 μs. The calculations indicate that both parallel and perpendicular ($1/2\rightarrow -1/2$) transitions to $X_1\ ^2\Pi_{1/2}$ are predominantly responsible for the observed intensity, with a partial lifetime of 1.2 μs arising on this basis. The transition probabilities are approximately equal for each of the three electric dipole moment components. By contrast, the $B-X_2$ partial lifetime is 9.0 μs, so that the total B lifetime is computed to be 1.1 μs, about double the measured value.[9]

The $C\ ^2\Delta_{3/2}$ state at slightly higher energy (Table IV) undergoes relatively strong perpendicular transitions to $X_1\ ^2\Pi_{1/2}$ as well as parallel transitions to X_2. The corresponding computed partial lifetimes of the $v'=0$ state are

1.59 and 1.02 μs, respectively (Table IV). The total C state radiative lifetime is thus found to be 0.68 μs, quite in agreement with the measured result[9] of 0.81 μs. Both theory and experiment thus find the $B-X$ and $C-X$ transitions to be relatively strong, consistent with the fact that these upper states were detected in early spectroscopic investigations.[6,19] There is also an indication on this basis that the agreement between the present calculated results and the corresponding measured values improve with the strength of the transitions being considered.

Finally, it will be recalled from Sec. III B that the best candidate for the observed $D\ ^2\Pi_{1/2}$ state[19] is computed to have a potential curve with a shoulder rather than a minimum in the Franck–Condon region of the ground state. Although no vibrational states could be obtained, it is still possible to estimate the radiative lifetime of the D state on the basis of strictly electronic wave function results. It is found that the corresponding Einstein coefficient decreases in going from $r=3.8a_0$, the X_1 r_e value, to $r=4.3a_0$ the approximate r_e value for other predominantly $\sigma^2\pi^3\pi^{*2}$ states. A lifetime in the 0.1–0.4 μs range is found on this basis, which suggests that the $D-X_1$ transitions are stronger than any of those discussed previously. No corresponding experimental result is as yet available. This result is at least consistent with the fact that the $D-X_1$ transition was discovered in early spectroscopic investigations[6,19] of the BiO system. In retrospect, it is somewhat surprising that the $K\ ^2\Sigma^+_{1/2}$ state was not detected earlier as well.

V. CONCLUSION

Relativistic CI calculations employing effective core potentials have been carried out for a large series of electronic states of bismuth oxide. Potential energy curves and transition probabilities have been computed with and without the inclusion of the spin–orbit coupling interaction. The lowest two electronic states are found to have predominantly $\sigma^2\pi^4\pi^*\ ^2\Pi$ character, but the next pair of higher-energy states are derived primarily from the $^4\Pi$ state of the $\sigma^2\pi^3\pi^{*2}$ configuration rather than one of the corresponding $^2\Pi$ species, contrary to earlier speculation. An interesting avoided crossing occurs between the $X_2\ ^2\Pi_{3/2}$ and $A_1\ ^4\Pi_{3/2}$ potential curves, and the resulting nonadiabatic effects are responsible for irregularities in vibrational progressions associated with these states. The $^4\Pi$ $\lambda-s$ species produces two other states with $\Omega=5/2$ and 1/2, respectively, which have thus far escaped experimental detection. The latter is predicted to undergo relatively strong parallel transitions to $X_1\ ^2\Pi_{1/2}$ and this fact might prove the basis for its eventual detection. The A_2 state has been known for some time and the calculations make this easily understandable by virtue of the relatively large transition probabilities it possesses to the X_1 ground state. The present computed lifetime of the A_2 state is 10.8 μs, which is in good agreement with the measured value of 9.3 μs. Unfortunately the agreement between theory and experiment is much less satisfactory in the case of the X_2-X_1 transition probability and the source of this error is not yet understood. The bond lengths of the X_1 and A_2 electronic states are overestimated in the present theoretical treatment by 0.11 and 0.06 Å, respectively, which errors are thought to be caused mainly by the choice of bismuth RECP employed and the lack of d-shell correlation effects in the present treatment. The corresponding T_e values for A_1 and A_2 are underestimated by 1200 and 1900 cm^{-1}, respectively.

The next group of low-lying states G through J are found to be composed of the $\sigma^2\pi^3\pi^{*2}$ and $\sigma\pi^4\pi^{*2}$ electronic configurations. Their T_e values are also underestimated in the present calculations, with errors falling in the 1500 cm^{-1} range compared to experiment. The computed radiative lifetimes are in reasonably good agreement with observed values, which are typically in the 15 μs range. No comparisons with measured bond lengths are as yet possible for any of these four states, but the corresponding vibrational frequencies are found to be too large in each case, with errors of 10–60 cm^{-1} occurring. Two states originating from the $\sigma^2\pi^3\pi^{*2}$ $L\ ^2\Phi$ $\lambda-s$ state are also found to lie in the neighborhood of the $J\ ^4\Sigma^-_{3/2}$ species, but they undergo only very weak transitions to lower-energy states and have thus far not been confirmed by experiment. Another state resulting from the $\sigma^2\pi^4\sigma^*$ configuration of $^2\Sigma^+_{1/2}$ symmetry which was first suggested by the present calculations has been detected by Shestakov *et al.*[9] and assigned as the K state, however. Its measured radiative lifetime of $\sim$2 μs fits in well with our computed value of 1.0 μs.

Three other states B, C, and D, which were known much earlier,[6,8,19] have also been clearly identified on the basis of the present work. In all three cases, a strong perturbation is found, beginning at $r=4.3a_0$, which appears to be responsible for the fact that only a few vibrational levels have been observed for these states. Their T_e values are again underestimated by 1000–1500 cm^{-1} and the corresponding bond distances are computed to be too large by roughly 0.1 Å in each case. The B state was originally characterized as $^4\Sigma^-_{1/2}$, but the present study indicates that a $^2\Sigma^-_{1/2}$ assignment is the correct one. Each of the above three states is computed to have a radiative lifetime on the order of 1.0 μs. Observed values for the B and C states are consistent with these predictions (0.55 and 0.81 μs, respectively). Altogether it can be concluded that the present spin–orbit coupling CI treatment based on RECPs gives a sufficiently accurate description of details of the BiO spectrum to be helpful to experimentalists in making their assignments. A number of predictions are still unconfirmed, however, involving states coming from the $\sigma^2\pi^3\pi^*$ $A\ ^4\Pi$ or $L\ ^2\Phi$ $\lambda-s$ species.

ACKNOWLEDGMENTS

The authors are very grateful for numerous discussions with Professor E. H. Fink and Dr. O. D. Shestakov during the course of the present study. Special thanks are also due to Professor R. M. Pitzer for making available his ECP spin–orbit integral program to us. This work was supported in part by the Deutsche Forschungsgemeinschaft in the form of a Forschergruppe grant. The financial support of the Fonds der Chemischen Industrie is also hereby gratefully acknowledged. One of us (A.B.A.) thanks the Alexander von Humboldt Foundation for the granting of a stipend.

[1] P. A. Christiansen, Y. S. Lee, and K. S. Pitzer, J. Chem. Phys. **71**, 4445 (1979).
[2] W. C. Ermler, Y. S. Lee, P. A. Christiansen, and K. S. Pitzer, Chem. Phys. Lett. **81**, 70 (1981).
[3] P. A. Christiansen, K. Balasubramanian, and K. S. Pitzer, J. Chem. Phys. **76**, 5087 (1982).
[4] A. B. Alekseyev, H.-P. Liebermann, I. Boustani, G. Hirsch, and R. J. Buenker, Chem. Phys. **173**, 333 (1993).
[5] A. B. Alekseyev, R. J. Buenker, H.-P. Liebermann, and G. Hirsch, J. Chem. Phys. **100**, 2989 (1994).
[6] K. P. Huber and G. Herzberg, *Molecular Spectra and Molecular Structure* (Van Nostrand–Reinhold, Princeton, NJ, 1979), Vol. 4.
[7] R. Mecke and M. Guillery, Phys. Z. **28**, 514 (1927).
[8] S. B. Rai and D. K. Rai, Chem. Rev. **84**, 73 (1984).
[9] O. Shestakov, R. Breidohr, H. Demes, K. D. Setzer, E. H. Fink, and W. Zyrnicki (private communication).
[10] P. A. Christiansen, Chem. Phys. Lett. **109**, 145 (1984).
[11] R. B. Ross, J. M. Powers, T. Atashroo, W. C. Ermler, L. A. LaJohn, and P. A. Christiansen, J. Chem. Phys. **93**, 6654 (1990).
[12] L. F. Pacios and P. A. Christiansen, J. Chem. Phys. **82**, 2664 (1985).
[13] W. H. E. Schwarz and R. J. Buenker, Chem. Phys. **13**, 153 (1976).
[14] R. J. Buenker and S. D. Peyerimhoff, Theor. Chim. Acta **35**, 33 (1974); **39**, 217 (1975); R. J. Buenker, S. D. Peyerimhoff, and W. Butscher, Mol. Phys. **35**, 771 (1978).
[15] R. J. Buenker and R. A. Phillips, J. Mol. Struct. Theochem. **123**, 291 (1985).
[16] E. R. Davidson, in *The World of Quantum Chemistry*, edited by R. Daudel and B. Pullman (Reidel, Dordrecht, 1974), p. 17.
[17] G. Hirsch, P. J. Bruna, S. D. Peyerimhoff, and R. J. Buenker, Chem. Phys. Lett. **52**, 442 (1977); D. B. Knowles, J. R. Alvarez-Collado, G. Hirsch, and R. J. Buenker, J. Chem. Phys. **92**, 585 (1990).
[18] J. W. Cooley, Math. Comput. **15**, 363 (1961).
[19] R. F. Barrow, W. J. M. Gissane, and D. Richards, Proc. R. Soc. London Ser. A **300**, 469 (1967); W. J. M. Gissane and R. F. Barrow, Proc. R. Soc. **85**, 1048 (1965); **86**, 682 (1965).
[20] A. Macias and A. Riera, J. Phys. B **11**, L489 (1978).
[21] C. Petrongolo, G. Hirsch, and R. J. Buenker, Mol. Phys. **70**, 825 (1990); G. Hirsch, R. J. Buenker, and C. Petrongolo, *ibid.* **70**, 835 (1990).
[22] Y. Li, M. Honigmann, K. Bhanuprakash, G. Hirsch, R. J. Buenker, M. A. Dillon, and M. Kimura, J. Chem. Phys. **96**, 8314 (1992).
[23] M. Eilers, Ph.D. dissertation, Bergische Universität, Wuppertal, Germany.